Journal of Photochemistry & Photobiology, B: Biology 158 (2016) 136–144

Contents lists available at ScienceDirect

Journal of Photochemistry & Photobiology, B: Biology

journal homepage: www.elsevier.com/locate/jphotobiol

Scrutinizing the DNA damaging and antimicrobial abilities of triazole appended metal complexes

Ponnukalai Ponya Utthra, Narayanaperumal Pravin, Natarajan Raman *

Research Department of Chemistry, VHNSN College, Virudhunagar 626 001, India

ARTICLE INFO

Article history:
Received 12 January 2016
Received in revised form 9 February 2016
Accepted 11 February 2016
Available online 4 March 2016

Keywords:
Fluorescence
Intercalation
Triazole analogues
DNA binding
Antimicrobial activity

ABSTRACT

New mononuclear transition metal complexes **1**–**12** bearing the bioactive triazole analogues were synthesized and characterized by elemental analysis and spectroscopic techniques. The interaction of calf thymus DNA (CT-DNA) with the synthesized compounds was studied at physiological pH by spectrophotometric, spectrofluorometric, cyclic voltammetry, and viscometric techniques. The entire DNA binding results suggested the intercalative mode of binding for the synthesized compounds. Interestingly, the binding strength of the complexes is found to be greater than that of the free ligands. Among the complexes explored, complex **5** reveals strong hypochromism and a slight red shift as compared to the other complexes highlighting its higher DNA binding propensity. The intrinsic binding constant values of the complexes compared to cisplatin reveal that all the complexes are greater in magnitude than that of cisplatin. Fluorescence titrations show that the Cu(II) complexes have the ability to displace DNA-bound ethidium bromide. Also, these compounds induce cleavage in pBR322 plasmid DNA as indicated in gel electrophoresis and exhibit excellent nuclease activity in the presence of H_2O_2. Moreover, the complexes were screened for *in vitro* antimicrobial activity along with free ligands and solvent control. The outcome is that the complexes possess good activity than the free ligands. These complexes may have further scope in developing them into antimicrobial drugs and DNA probes.

1. Introduction

With the rapid spurt of exacerbated genetic disorders and diseases, damaging nucleic acids (DNA) have become a common drug target for the scientists and researchers. It is modified or damaged using various new generation drugs, metal complexes being one of them. To manipulate DNA for the desired results, metal complexes which can efficiently bind and cleave DNA under physiological conditions are considered as prospective candidates for use as therapeutic agents in medicinal applications and for genomic research [1–6]. The availability of various binding sites in DNA results in the interactions such as intercalation or groove binding or π–π interaction or electrostatic interaction between these small molecules and DNA. Among the binding modes intercalative binding, as most commonly studied, is the non-covalent stacking interaction resulting from the unwinding of the base pairs of DNA, to make way for the insertion of a planar heterocyclic aromatic ring between the DNA double helix.

Study of transition metals with organic ligands (Schiff based) has become a point of curiosity due to their intriguing structural features and potential application in various fields. Chelation to metal ions may lead to imperative changes in bioavailability and bioactivity of organic compounds that in turn could promote attractive enhancement in their overall biological performance [7]. In fact, the biological behavior of metal-based compounds is not only determined by the nature of the bioactive ligand but also by the nature and oxidation state of the metal centre and the electronic and physicochemical properties of the whole complex that is highly dependent on the availability of the donor atoms. These features, when modified, would allow the fine-tuning of important biological properties.

On the other hand, triazoles are structurally important precursors for obtaining various Schiff bases that have well-known antimicrobial properties [8,9]. Even though many triazoles are available, the 1,2,4-triazole nucleus and its derivatives emerge rapidly with the advance modern heterocyclic chemistry, promising a variety of therapeutic applications such as antifungal [10–12], antibacterial [13–15], antitumor [16,17], antiviral [18], anti-inflammatory [19], anti-asthmatic [20], anticonvulsant [21] plant growth-regulating [22] and cytotoxic [23] activities. Recently, few Schiff bases derived from 3-substituted-4-amino-5-mercapto-1,2,4-triazoles showed analgesic, antimicrobial, anti-inflammatory and antidepressant activities [24].

Bearing in mind the above facts, we herein report the synthesis, characterization, DNA binding, DNA cleavage (in the presence of H_2O_2) and antimicrobial studies of a series of novel octahedral complexes containing triazole analogues which were condensed from 3-amino,1,2,4-triazole and salicylaldehyde with Cu(II), Co(II), Ni(II) and

* Corresponding author.
E-mail address: ramchem1964@gmail.com (N. Raman).

http://dx.doi.org/10.1016/j.jphotobiol.2016.02.033
1011-1344/

Zn(II) metal ions. The results showed promise in designing and developing newer and effective antimicrobial agents as well as novel DNA probes.

2. Experimental Protocol

The materials and methods, DNA binding, cleavage and antimicrobial procedures are given in the Supplementary file (S1).

2.1. Synthesis of Schiff Bases (L^1–L^3)

The Schiff bases (**L^1**–**L^3**) were prepared by condensing of 3-amino-1,2,4-triazole (10 mmol) dissolved in hot ethanol (15 mL) to a magnetically stirred hot solution of salicylaldehyde and its derivatives (where **L^1** — salicylaldehyde derived Schiff base, **L^2** — nitro substituted salicylaldehyde derived Schiff base, **L^3** — methoxy substituted salicylaldehyde derived Schiff base) (10 mmol) in hot ethanol (15 mL). The condensed mixture was then refluxed for 2 h and the yellow solid precipitated on cooling was washed with hot ethanol first, then pet-ether and dried. Further, it was recrystallized in a hot solution of ethanol–methanol (1:1) and dried *in vacuo*. The same method was applied for the preparation of all other ligands **L^2** and **L^3**.

[L^1], Yield: 72%. Anal. calc. for $C_9H_8N_4O$: C, 57.4; H, 4.2; N, 29.7%; Found C, 57.3; H, 4.1; N, 29.5%. IR data (KBr, cm^{-1}); 1645 ν(C═N), 3172 (—NH triazole ring), 3363 (H-bonded OH), 1575–1400 (C═C aromatic stretching), 1047 (N—N bond of triazole). ^{1}H NMR (δ, ppm): 7.02–7.63 (aromatic) (m); 8.5 (CH) (s), 8.2 (CH) (s), 5.3 (OH) (s), 13.5 (—NH) (s). ^{13}C NMR (δ, ppm): 120.5–132.1 (C_1 to C_6), 160.0 (C_7), 158.1 (C_8), 146.6 (C_9). UV–vis, (DMF, cm^{-1}); 35,998, 27,361. MS m/z (%): 188 [M^+].

[L^2], Yield: 74%. Anal. calc. for $C_9H_7N_5O_3$: C, 46.3; H, 3.0; N, 30.0%; Found C, 46.2; H, 2.9; N, 29.8%. IR data (KBr, cm^{-1}); 1643 ν(C═N), 3196 (—NH triazole ring), 3298 (H-bonded OH), 1575–1400 (C═C aromatic stretching), 1047 (N—N bond of triazole), 1473, 1312, 833 ν(—C—N str; —NO_2). ^{1}H NMR (δ, ppm): 7.28–8.35 (aromatic) (m); 8.3 (CH) (s), 8.2 (CH) (s), 5.3 (OH) (s), 13.5 (—NH) (s). ^{13}C NMR (δ, ppm): 118.0–140.6 (C_1 to C_6), 160.0 (C_7), 158.1 (C_8), 146.6 (C_9). UV–vis, (DMF, cm^{-1}); 35,985, 28,601. MS m/z (%): 233 [M^+].

[L^3], Yield: 70%. Anal. calc. for $C_{10}H_{10}N_4O_2$: C, 55.0; H, 4.6; N, 25.6%; Found C, 54.9; H, 4.5; N, 25.4%. IR data (KBr, cm^{-1}); 1638ν(C═N), 3187 (—NH triazole ring), 3324 (H-bonded OH), 1575–1400 (C═C aromatic stretching), 1047 (N—N bond of triazole). ^{1}H NMR (δ, ppm): 6.91–7.33 (aromatic) (m); 8.3 (CH) (s), 8.2 (CH) (s), 5.3 (OH) (s), 13.5 (—NH) (s); 3.8 (—OCH_3) (s). ^{13}C NMR (δ, ppm): 113.5–153.3(C_1 to C_6), 160.0 (C_7), 158.1 (C_8), 146.6 (C_9), 55.8 (C_{10}). UV–vis, (DMF, cm^{-1}); 39,651, 29,149. MS m/z (%): 218 [M^+].

2.2. Synthesis of Metal Complexes

The metal complexes of the types [$M(L^1)_2$], [ML^1L^2] and [ML^1L^3] were synthesized using the following procedure. The synthesized ligand L^1 (20 mmol) was dissolved in a hot ethanolic solution and condensed with the appropriate metal chloride salts (Cu, Co, Ni, Zn) (10 mmol). On cooling the product obtained was washed with hot ethanol, pet-ether and then dried *in vacuo*. The obtained metal complexes [$M(L^1)_2$] were in 1:2 ratio (metal: L^1). Similar procedure was followed for the preparation of other metal complexes, where the metal ratios were the same while the ratios of ligands were varied. Accordingly, complexes **5–8** were of type [ML^1L^2] with (L^1:M:L^2) ratio and complexes **9–12** were of type [ML^1L^3] with the ratio (L^1:M:L^3).

[$Cu(L^1)_2$] (**1**), Yield: 78%, Anal. calc. for $C_{18}H_{14}CuN_8O_2$: C, 49.3; H, 3.2; N, 25.5; Cu, 14.5%; Found C, 49.1; H, 3.1; N, 25.3; Cu, 14.2%. IR data (KBr, cm^{-1}); 1607 ν(C═N), 3413 (—NH triazole ring), 425 ν(M—N), 574 ν(M—O). MS m/z (%): 437 [M^+]. Λ_M 10^{-3} (Ω^{-1} cm^2 mol^{-1}) = 14.6.λ_{max} (cm^{-1}) in DMF, 15,997,14,861,15,345. μ_{eff} (BM): 1.84.

[$Co(L^1)_2$] (**2**) Yield: 75%, Anal. calc. for $C_{18}H_{14}CoN_8O_2$: C, 49.9; H, 3.2; N, 25.8; Cu, 13.6%; Found C, 49.7; H, 3.1; N, 25.6; Co, 13.4%. IR data (KBr, cm^{-1}); 1603 ν(C═N), 3172 (—NH triazole ring), 427 ν(M—N), 554 ν(M—O). MS m/z (%): 433 [M^+]. Λ_M 10^{-3} (Ω^{-1} cm^2 mol^{-1}) = 15.3. λ_{max} (cm^{-1}) in DMF, 10,800, 10,941, 27,648. μ_{eff} (BM): 4.85.

[$Ni(L^1)_2$] (**3**) Yield: 76%, Anal. calc. for $C_{18}H_{14}N_8NiO_2$: C, 49.9; H, 3.2; N, 25.8; Ni, 13.5%; Found C, 49.8; H, 3.0; N, 25.4; Ni, 13.3%. IR data (KBr, cm^{-1}); 1605 ν(C═N), 3172 (—NH triazole ring), 431 ν(M—N), 561 ν(M—O). MS m/z (%): 432 [M^+]. Λ_M 10^{-3} (Ω^{-1} cm^2 mol^{-1}) = 15.6. λ_{max} (cm^{-1}) in DMF, 10,940, 10,100, 27,413. μ_{eff} (BM): 3.15.

[$Zn(L^1)_2$] (**4**) Yield: 73%, Anal. calc. for $C_{18}H_{14}N_8O_2Zn$: C, 49.1; H, 3.2; N, 25.4; Zn, 14.8%; Found C, 49.0; H, 3.1; N, 25.2; Zn, 14.7%. IR data (KBr, cm^{-1}); 1608 ν(C═N), 3172 (—NH triazole ring), 428 ν(M—N), 572 ν(M—O). MS m/z (%): 438 [M^+]. ^{1}H NMR (δ, ppm): 7.01–7.66 (aromatic) (m); 8.6 (CH) (s), 8.3 (CH) (s), 13.5 (—NH) (s). ^{13}C NMR (δ, ppm): 116.2–157.8 (C_1 to C_6), 157.8 (C_7), 157.5 (C_8), 145.7 (C_9). Λ_M 10^{-3} (Ω^{-1} cm^2 mol^{-1}) = 14.7. λ_{max} (cm^{-1}) in DMF, 39,589, 27,489. μ_{eff} (BM): diamagnetic.

[CuL^1L^2] (**5**) Yield: 77%, Anal. calc. for $C_{18}H_{13}CuN_9O_4$: C, 44.7; H, 2.7; N, 26.1; Cu, 13.1%; Found C, 44.5; H, 2.4; N, 26.0; Cu, 13.0%. IR data (KBr, cm^{-1}); 1610 ν(C═N), 3196 (—NH triazole ring), 434 ν(M—N), 592 ν(M—O). MS m/z (%): 482 [M^+]. Λ_M 10^{-3} (Ω^{-1} cm^2 mol^{-1}) = 19.5.λ_{max} (cm^{-1}) in DMF, 15,890, 14,435, 15,726. μ_{eff} (BM): 1.86.

[CoL^1L^2] (**6**) Yield: 72%, Anal. calc. for $C_{18}H_{13}CoN_9O_4$: C, 45.2; H, 2.7; N, 26.3; Co, 12.3%; Found C, 45.0; H, 2.6; N, 26.1; Co, 12.1%. IR data (KBr, cm^{-1}); 1606 ν(C═N), 3196 (—NH triazole ring), 421 ν(M—N), 587 ν(M—O). MS m/z (%): 478 [M^+]. Λ_M 10^{-3} (Ω^{-1} cm^2 mol^{-1}) = 17.2.λ_{max} (cm^{-1}) in DMF, 10,118,11,341,24,930. μ_{eff} (BM): 4.88

[NiL^1L^2] (**7**) Yield: 79%, Anal. calc. for $C_{18}H_{13}N_9NiO_4$: C, 45.2; H, 2.7; N, 26.3; Ni, 12.2%; Found C, 45.1; H, 2.5; N, 26.1; Ni, 12.1%. IR data (KBr, cm^{-1}); 1603 ν(C═N), 3196 (—NH triazole ring), 433 ν(M—N), 575 ν(M—O). MS m/z (%): 477 [M^+]. Λ_M 10^{-3} (Ω^{-1} cm^2 mol^{-1}) = 18.5. λ_{max} (cm^{-1}) in DMF, 11,411,10,040, 25,113. μ_{eff} (BM):3.10.

[ZnL^1L^2] (**8**) Yield: 75%, Anal. calc. for $C_{18}H_{13}N_9O_4Zn$: C, 44.6; H, 2.7; N, 26.0; Zn, 13.4%; Found C, 44.5; H, 2.6; N, 25.9; Zn, 13.2%. IR data (KBr, cm^{-1}); 1609 ν(C═N), 3196 (—NH triazole ring), 429 ν(M—N), 562 ν(M—O). MS m/z (%): 483 [M^+]. ^{1}H NMR (δ): 7.04–7.58 (aromatic) (m); 8.5 (CH) (s), 8.3 (CH) (s), 13.5 (—NH) (s). ^{13}C NMR (δ, ppm): 115.8–157.9 (C_1 to C_6), 157.2 (C_7), 157.3 (C_8), 145.2 (C_9). Λ_M 10^{-3} (Ω^{-1} cm^2 mol^{-1}) = 16.9.λ_{max} (cm^{-1}) in DMF, 35,668, 28,972. μ_{eff} (BM): diamagnetic.

[CuL^1L^3] (**9**) Yield: 71%, Anal. calc. for $C_{19}H_{16}CuN_8O_3$: C, 48.7; H, 3.4; N, 23.9; Cu, 13.5%; Found C, 48.5; H, 3.3; N, 23.7; Cu, 13.4%. IR data (KBr, cm^{-1}); 1611 ν(C═N), 3187 (—NH triazole ring), 436 ν(M—N), 595 ν(M—O). MS m/z (%): 467 [M^+]. Λ_M 10^{-3} (Ω^{-1} cm^2 mol^{-1}) = 14.2. λ_{max} (cm^{-1}) in DMF, 15,637, 14,741,15,878. μ_{eff} (BM): 1.89.

[CoL^1L^3] (**10**) Yield: 70%, Anal. calc. for $C_{19}H_{16}CoN_8O_3$: C, 49.2; H, 3.4; N, 24.1; Co, 12.7%; Found C, 49.1; H, 3.3; N, 24.0; Co, 12.6%. IR data (KBr, cm^{-1}); 1607 ν(C═N), 3187 (—NH triazole ring), 426 ν(M—N), 567 ν(M—O). MS m/z (%): 463 [M^+]. Λ_M 10^{-3} (Ω^{-1} cm^2 mol^{-1}) = 15.8. λ_{max} (cm^{-1}) in DMF, 10,451, 11,427, 26,348. μ_{eff} (BM): 4.82

[NiL^1L^3] (**11**) Yield: 68%, Anal. calc. for $C_{19}H_{16}N_8NiO_3$: C, 49.2; H, 3.4; N, 24.2; Ni, 12.6%; Found C, 49.1; H, 3.3; N, 24.1; Ni, 12.5%. IR data (KBr, cm^{-1}); 1604 ν(C═N), 3187 (—NH triazole ring), 435 ν(M—N), 592 ν(M—O). MS m/z (%): 462 [M^+]. Λ_M 10^{-3} (Ω^{-1} cm^2 mol^{-1}) = 18.7. λ_{max} (cm^{-1}) in DMF, 11,910, 10,163, 25,715. μ_{eff} (BM): 3.17.

[ZnL^1L^3] (**12**) Yield: 73%, Anal. calc. for $C_{19}H_{16}N_8O_3Zn$: C, 48.5; H, 3.4; N, 23.8; Zn, 13.5%; Found C, 48.3; H, 3.3; N, 23.7; Zn, 13.5%. IR data (KBr, cm^{-1}); 1605 ν(C═N), 3187 (—NH triazole ring), 423 ν(M—N), 587 ν(M—O). MS m/z (%): 468 [M^+]. ^{1}H NMR (δ): 7.1–7.9 (aromatic) (m); 8.4 (CH) (s), 8.3 (CH) (s), 13.5 (—NH) (s). ^{13}C NMR (δ, ppm): 116.0–158.9 (C_1 to C_6), 157.6 (C_7), 158.9 (C_8), 146.2 (C_9), 55.8 (C_{10}). Λ_M 10^{-3} (Ω^{-1} cm^2 mol^{-1}) = 16.2. λ_{max} (cm^{-1}) in DMF, 35,425, 28,943. μ_{eff} (BM): diamagnetic.

3. Results and Discussion

The synthetic pathways of the formation of Schiff bases and their complexes are drafted in Scheme 1. The ligands and their complexes are found to be stable in air. The ligands are soluble in common organic solvents but their complexes are soluble only in DMF and DMSO.

3.1. Elemental Analysis and Molar Conductivity Measurements

The results of elemental analysis for the metal complexes are in good agreement with the calculated values showing that the complexes (**1**–**4**) have 1:2 ratio (metal:L^1) of the type $[M(L^1)_2]$, complexes (**5**–**8**) have 1:1:1 ratio (L^1:M:L^2) of the type $[ML^1L^2]$ and complexes (**9**–**12**) have 1:1:1 ratio (L^1:M:L^3) of the type $[ML^1L^3]$, wherein the $\mathbf{L^1}$, $\mathbf{L^2}$ and $\mathbf{L^3}$ act as tridentate ligands. The complexes are found to be non-electrolytic nature (14.2–19.5 Ω^{-1} cm^2 mol^{-1}) in 10^{-3} M DMF solution, implying the replacement of chloride anions by hydroxyl group to the metal ion [25]. The absence of counter (chloride) ions is confirmed from Volhard's test.

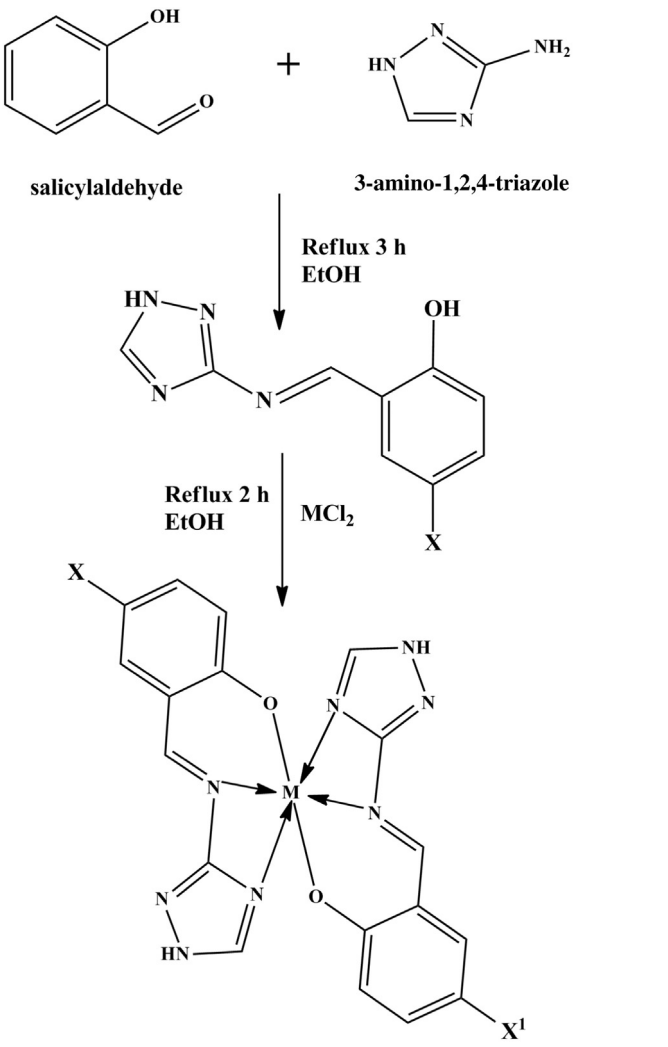

Scheme 1. Synthesis of Schiff base ligands and their metal complexes.

3.2. IR Spectra

The formation of the compounds has been ascertained by the comparison of the IR spectra of the ligands and their complexes. The bands corresponding to the azomethine group ν(—CH═N) at the region 1639–1645 cm^{-1} in the spectra of the free ligands were considerably shifted to lower frequencies ~1603–1611 cm^{-1} in the complexes, indicating the involvement of the azomethine nitrogen in the coordination with the metal ion, which was further supported by the appearance of new bands in their spectra at 421–436 cm^{-1}, assigned to the ν(M—N) stretching vibrations. The spectra of the ligands revealed a broad envelope in the 3298–3363 cm^{-1} region, assigned to the —OH group, which was found absent in complexes indicating the deprotonation of the hydroxyl group upon coordination to the metal ions [26]. Sharp peak in the range 3172–3196 cm^{-1} belonging to the —NH of triazole appeared in all the ligands and complexes, signifying its non-participation in the complexation. The presence of medium intensity bands at 595–550 cm^{-1} corresponding to ν(M—O), further confirmed the proposed structure.

3.3. Electronic Spectra and Magnetic Properties of the Complexes

With the view to assign the stereochemistry of metal ions in the complexes based on the position and number of d–d transition peaks, the electronic spectral data of Cu(II), Co(II), Ni(II) and Zn(II) complexes of the ligands $\mathbf{L^1}$–$\mathbf{L^3}$ were recorded in DMF. The free ligands exhibited two intense bands in the 35,985–39,651 and 27,361–29,149 cm^{-1} regions due to $\pi \rightarrow \pi^*$ and $n \rightarrow \pi^*$ transitions [27], respectively. In all the metal complexes, the absorption bands at 35,803–39,498 and 27,340–29,140 cm^{-1} are due to $\pi \rightarrow \pi^*$ and $n \rightarrow \pi^*$ transitions that are observed in the spectra of the free ligands $\mathbf{L^1}$–$\mathbf{L^3}$. These transitions were shifted to higher or lower frequencies due to the coordination of the ligand with metal ions.

The electronic spectra of the Cu(II) complexes (**1**, **5** and **9**) showed absorption bands in the range 15,890–14,741 cm^{-1} assigned to transitions $^2E_g \rightarrow {}^2T_{2g}$. These data reveal that complexes **1**, **5** and **9** adopt a distorted octahedral geometry around the central metal ion. The magnetic moment observed for these complexes was found to be in the range 1.84–1.89 BM which indicates that the mononuclear complexes are uncoupled d^9 systems with an $s = 1/2$ spin state of distorted octahedral geometry [28]. Furthermore, the microanalytical data and mass spectral data second the monomeric nature of the complexes. Three d–d bands were displayed by Co(II) complexes (**2**, **6** and **10**) which were found in the region 10,118–27,648 cm^{-1} and assigned to $^4T_{2g}$ (F) $\rightarrow {}^4T_{2g}$(F), $^4T_{1g}$ (F) $\rightarrow {}^4A_{2g}$(F) and $^4T_{1g}$ (F) $\rightarrow {}^4T_{2g}$(P) which revealed the octahedral geometry of the complexes. Their monomeric nature was indicated by the observed magnetic moments of the complexes (**2**, **6** and **10**) in the range 4.82–4.88 BM, at room temperature along with the confirmation by microanalytical data. The electronic spectra of the Ni(II) complexes (**3**, **7** and **11**) showed three low intensity bands in the region around 10,040–27,413 cm^{-1}, assigned to $^3A_{2g}$(F) $\rightarrow {}^3T_{2g}$(F), $^3A_{2g}$(F) $\rightarrow {}^3T_{1g}$(F) and $^3A_{2g}$(F) $\rightarrow {}^3T_{1g}$(P) suggesting that the Ni(II) ion is surrounded in an octahedral geometry. The observed magnetic moment of the complexes (**3**, **7** and **11**) were at the range of 3.10–3.17 BM at room temperature indicating uncoupled mononuclear complexes of a diluted d^8 system with an $s = 1$ spin state of octahedral geometry [29,30].The monomeric nature of the complexes (**3**, **7** and **11**) was further supported by microanalytical data. The electronic absorption spectra for the diamagnetic Zn(II) complexes(**4**, **8** and **12**) showed bands in the region 34,602–28,498 cm^{-1} which were assigned to intraligand charge-transfer transitions [31]. According to the empirical formulae, an octahedral geometry is proposed for Zn(II) complexes.

3.4. ^{1}H NMR Spectra

The NMR spectrum is exploited to determine the identity of prepared ligands and their diamagnetic metal complexes. The spectra of

free ligands show peaks at 6.9–8.3 ppm which is attributed to phenyl multiplet. The free ligands also showed the following signals: for —NH 13.5 ppm (s), for —OH at 5.3 ppm, —CH═N 8.3–8.5 ppm. The signals of the azomethine proton of free ligands were shifted to 7.1–7.9 ppm in the Zn(II) complexes (**4**, **8** and **12**), a downfield shift, which suggests deshielding of azomethine group thereby confirming the coordination of the metal ion with the azomethine. The disappearance of hydroxyl proton signals in the Zn(II) complexes suggests its involvement in the chelation. The other proton frequencies and their Zn(II) complexes did not show any appreciable changes.

3.5. ^{13}C NMR Spectra

The ^{13}C NMR of the free ligands showed signals at 113.5–153.3 ppm corresponding to salicylaldehyde moiety. The signals of the carbons of the triazole moiety for the free ligands were found at 146.6 ppm and 158.1 ppm respectively. In the free ligand L^3, the signal of —OCH_3 was found at 55.8 ppm which also appeared in all the Zn(II) complexes (**4**, **8** and **12**), clearly indicating that it does not participate in the complexation. The azomethine region of the free ligands was observed at 160 ppm, whereas in the spectra of Zn(II) complexes, an upfield shift was observed depicting a signal at 157 ppm. Therefore, the above data confirms the participation of azomethine group in the coordination. No noticeable changes were found in the other signals.

3.6. Electron Paramagnetic Spectrum of the Cu(II) Complexes

The EPR spectra of Cu(II) complexes were recorded in DMSO at 300 K and 77 K. The spin Hamiltonian parameters of the complexes have been calculated and are summarized in Table 1. From this spectral data, it is found that $A_{||}$ (107–113) > $A_{\perp}$(121–128); $g_{||}$ (2.21–2.29) > $g_{\perp}$(2.05–2.06) > g_e(2.0023), which support the d^2_{x-y} as the ground state, characteristic of octahedral geometry and axially symmetric. Further, in an axial symmetry, the g-values are related by the expression, $G = (g_{||} - 2)/(g_{\perp} - 2)$, which measures the exchange interaction between the copper centers in polycrystalline solid. The G values lie within the range 4.35–4.99 for all the copper complexes indicating negligible exchange interaction of Cu–Cu in the complexes according to Hathaway [32]. These values were further supported by their magnetic moment values for complexes **1**, **5** and **9** as 1.84, 1.86 and 1.89 BM, respectively.

Apart from this, the covalency parameter (α^2) has been calculated using Kivelson and Neiman equations [33]. The covalency parameter ($\alpha^2 = 0.81$–0.99) indicates considerable covalent character for the metal–ligand bond. Thus, the spectral data discussed above confirm the proposed structure of Cu(II) complexes and is depicted in Fig. 1.

3.7. Mass Spectra

The Schiff base ligands **L^1**–**L^3** and their Cu(II) metal complexes were subjected to the ESI-Mass spectral analysis to further confirm their proposed stoichiometry. The spectrum of L^1 showed a molecular ion peak $[M^+]$ at m/z = 188 equivalent to its molecular weight, corresponding to its molecular formula, $C_9H_8N_4O$. In addition to this, the fragmentation peaks observed at m/z 96, 69 and 29 are due to the cleavage of $[C_3H_3N_4]^+$, $[C_2H_2N_3]^+$, and $[CH_2N]^{2+}$ respectively. The results confirm the formation of Schiff base **L^1** supporting the IR and NMR results and its Cu(II) complex **1** showed a molecular ion $[M^+]$ at m/z 437, equivalent to its molecular weight having the formula $C_{18}H_{14}C_4N_8O_2$. Thus, the mass spectral data results along with elemental analyses data agree with the formation of $[M(L^1)_2]$ type complexes of 1:2 stoichiometry. Similarly, the mass spectrum of Schiff base **L^2** showed a molecular ion peak $[M^+]$ at m/z = 233, equivalent to its molecular weight, corresponding to its molecular formula $C_9H_7N_5O_3$. The fragmentation peaks observed at m/z 96, 69 and 29 are due to the cleavage of $[C_3H_3N_4]^+$, $[C_2H_2N_3]^+$, and $[CH_2N]^{2+}$ respectively. The results confirmed the formation of Schiff base L^2 supporting the IR and NMR results and its Cu(II) complex **5** showed a molecular ion $[M^+]$ at m/z 482, equivalent to its molecular weight having the formula $C_{18}H_{13}CuN_9O_4$. Thus, the mass spectral data results along with elemental analyses data agree well that the complexes are of 1:1:1 ratio and the type $[ML^1L^2]$.

3.8. DNA Binding Studies

3.8.1. Absorption Spectral Titrations

DNA, being the most favored intracellular target, alters the nature of the cell when manipulated. These alterations may be achieved by the binding or tethering of the suitable metal complexes into the helix of the DNA. Among the different modes of binding such as covalent, non-covalent and electrostatic binding, non-covalent binding nature of the complexes is much preferred. When the metal complexes find its way into the helix of the DNA along the groove, groove binding (non covalent binding) is the outcome. In the same manner, when the path of the metal complexes is through the base pairs of DNA, intercalation takes place. Therefore, most of the DNA binders are metal complexes that contain ligands which are able to π-stack between base pairs of DNA. The consequences of these DNA binding phenomenon is the much required kinking, unwinding or bending of the DNA helix. Hence, the studies on ability of complexes to potentially bind to DNA have provided a clue of paramount importance for the development of effective metal-based chemotherapeutic drugs.

Electronic absorption spectroscopy is an efficient method of examining the mode and extent of binding of a metal complex with DNA, based on which the free ligands L^1–L^3 and their complexes (**1**–**12**) were analyzed by comparing the spectral data in the presence and absence of the CT-DNA. The absorption spectra of complexes **3** and **5** in the absence and presence of CT DNA at different concentrations are shown in Fig. 2. The UV spectra of the free ligands showed intense absorption around 275–294 nm which is attributed to π–π* transition energies and their complexes exhibited an intense absorption around 272–296 nm. With the increasing concentration of DNA, both the ligands and their complexes showed hypochromicity and red shifted charge transfer peak maxima in the absorption peak spectra. In the case of ligands, the observed hypochromicity in the range 8.4–10.8% and slight red shift in the range 0.3–1 nm, can be seen in the absorption spectra. The hypochromicity values of all the complexes observed in the presence of DNA were in the range 13.5–29.9% and their red shifts were in the region 2–4 nm. The intrinsic binding values (K_b) for the complexes were evaluated by the change observed in the absorbance values with the increase in the DNA concentration, the values of which are displayed in Table 2.

The nature of the binding of the complexes with the DNA induces the change in hypochromicity, which is significant due to stacking or hydrophobic interactions of the aromatic ring [34]. However, the

Table 1
The spin Hamiltonian parameters of the Cu(II) complexes in DMSO solution at 77 K.

Complexes	g-Tensor			$A \times 10^{-4}$ (cm^{-1})			f	G	α^2	β^2	$K_{\perp}$	$K_{||}$
	$g_{||}$	$g_{\perp}$	g_{iso}	$A_{||}$	$A_{\perp}$	A_{iso}						
1	2.29	2.06	2.14	107	126	119	214	4.99	0.97	0.80	0.63	0.59
5	2.27	2.06	2.13	113	121	118	204	4.64	0.81	0.79	0.69	0.55
9	2.21	2.05	2.10	110	128	122	200	4.35	0.99	0.84	0.79	0.51

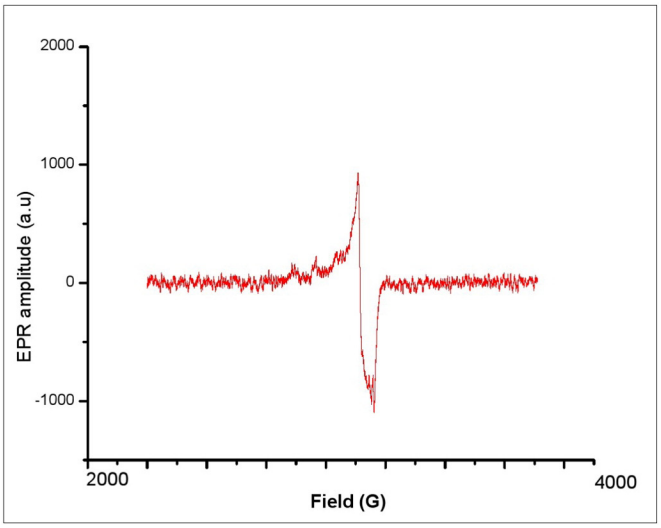

Fig. 1. X-band EPR spectrum of complex **5** at liquid nitrogen temperature (77 K).

metal ions play an influential role in DNA binding by these complexes. The binding strength of the complexes is shown as in the following order: **5** > **9** > **1** > **6** > **10** > **2** > **7** > **11** > **3** > **8** > **12** > **4**. Complex **5** reveals strong hypochromism and a slight red shift as compared to the other complexes highlighting its higher DNA binding propensity. The intrinsic binding constant values of the complexes compared to cisplatin (standard drug for cancer) revealed that all the complexes are greater in magnitude ($1.1–2.9 \times 10^5$) than that of cisplatin ($5.73 \pm 0.45 \times 10^4\ M^{-1}$) [35]. From the results, ligands themselves act as a feeble intercalator as compared to the complexes that act as strong intercalators. These results suggest that the intercalative ligands with extended aromatic plane, good conjugation effect and electron withdrawing substitution group can greatly promote the DNA binding ability.

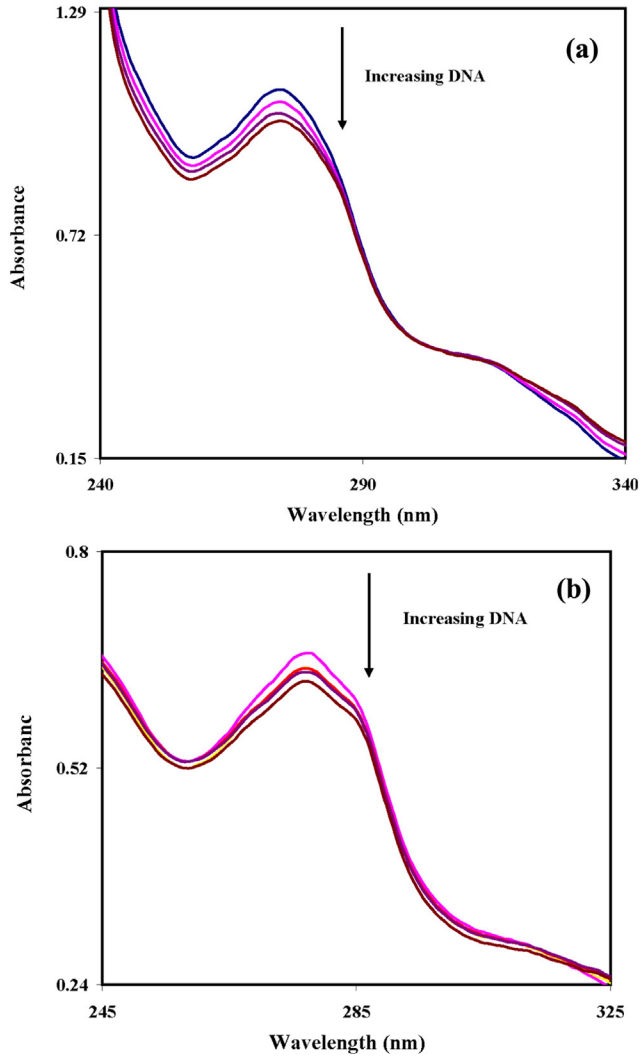

Fig. 2. Absorption spectra of complexes **3** (a) and **5** (b) in buffer pH = 7.2 at 25 °C in the presence of increasing amount of DNA.

3.8.2. Fluorescence Spectroscopic Studies

With the intention to further confirm the intercalative mode of binding, fluorescence titration has been accompanied with EB–DNA system. This technique has been extensively used to determine the mode of binding of these drugs to DNA because of its high sensitivity, good repeatability and accuracy. The intrinsic fluorescence intensity of DNA is very low and that of EB–Tris HCl buffer is also not high because of the quenching by the solvent molecules. It is already reported that EB can show enhanced emission intensity in the presence of DNA due to the strong intercalation between the adjacent base pairs [36]. The binding mode is appraised by regarding the local environment of the EB–DNA system (after addition of complex) through the change in emission intensity and shift in wavelength. The binding ability of the copper complexes **1**, **5** and **9** was assessed by the EB–DNA compound system. Fascinatingly, the incremental addition of complex to the EB–DNA system causes a palpable reduction or quenching in the fluorescence intensity indicating that complex **5** competes with the already intercalated EB, to bind with the DNA. Thus, the EB–DNA is helpful, in measuring the DNA proclivity of the complex and stacking interaction (intercalation) between adjacent DNA base pairs, on the basis of decrease of fluorescence as the result of EB displacement from a DNA sequence by a quencher. The fluorescence spectra of EB–DNA system quenched by **5** and **9** are depicted in Fig. 3. The quenching of EB bound to DNA by the title complex is further explored using the linear Stern–Volmer equation:

$$I_0/I = 1 + K_{SV}[Q]$$

where, I_0 and I are the fluorescence intensities in the absence and presence of quencher (metal complex), respectively; [Q] is the concentration of the quencher and K_{SV} is the Stern–Volmer quenching constant (slope of plot between I_0/I and [Q]). The binding constants (K_{SV}) for

Table 2
Electronic absorption spectral properties of synthesized compounds.

Complexes	λ_{max} (nm)		Δλ (nm)	[a]H%	[b]K_b (M^{-1})[c]
	Free	Bound			
L^1	294.0	294.3	0.3	8.4	0.2×10^3
L^2	275.0	276.0	1	10.8	0.7×10^3
L^3	282.0	282.5	0.5	9.3	0.5×10^3
1	293.0	296.0	3	24.0	2.5×10^5
2	296.0	299.0	3	19.7	2.0×10^5
3	276.0	278.0	2	17.2	1.6×10^5
4	279.0	281.0	2	13.5	1.1×10^5
5	272.0	276.0	4	29.9	2.9×10^5
6	276.0	279.0	3	20.3	2.3×10^5
7	272.0	275.0	3	18.5	1.9×10^5
8	272.0	274.0	2	16.4	1.4×10^5
9	284.0	287.0	3	24.3	2.7×10^5
10	288.0	291.0	3	19.9	2.2×10^5
11	288.0	290.0	2	17.6	1.7×10^5
12	286.0	288.0	2	14.1	1.3×10^5

[a] $H\% = [(A_{free} - A_{bound}) / A_{free}] \times 100\%$.
[b] K_b = Intrinsic DNA binding constant determined from the UV–vis absorption spectral titration.
[c] Error limit ±3%.

complexes **1**–**12** were calculated and found to be in the range 0.59–1.04 × 10^5. The results are consistent with the absorption spectral measurements.

3.8.3. Viscosity Measurements

Viscosity, one of the hydrodynamic measurement methods, is performed to confirm the mode of binding of the CT DNA with the metal complex, in the absence of crystallographic data. The increase in viscosity regards to the classical intercalative mode, whereas its decrease may be due to the non-classical intercalation. The lengthening of DNA strands is due to separation between the base pairs caused by metal complexes in the classical intercalation. Fascinatingly, the DNA gets kinked or bent due to the non classical intercalation. The groove binding of the metal complexes causes negligible changes to the viscosity of the DNA solution. The viscosity of the DNA solution increases with increasing ratio of the complexes to DNA. Ethidium bromide, the known DNA-intercalator increases the relative viscosity of DNA due to its strong intercalation. The effects of complexes together with the viscosity of DNA are shown in Fig. 4. Compared with EB, complexes exhibit minor increase in the relative viscosity of the CT DNA. The free ligands exhibit frail intercalation as compared with EB. This result further suggests intercalative binding mode of the complexes with DNA and also parallels with photophysical results. The viscosity study provides a strong evidence for intercalation.

3.8.4. Cyclic Voltammetry

The electrochemical investigations interaction between the metal complexes and DNA provides a useful complement to the methods of investigation such as UV–vis and CD spectroscopy [37].The electrochemical potential of the molecule will shift positively when the complex intercalates into DNA double helix, and it will shift into a negative direction, if the molecule is bound to DNA by groove binding [38, 39].Using cyclic voltammetry (CV), the electrochemical behavior of all the **12** complexes was studied before and after the addition of DNA and the cyclic voltammograms for complexes **5** and **9** are depicted in Fig. 5. The voltammetric parameters obtained for all the complexes with and without DNA are given in Table 3. On addition of CT DNA, complexes experienced a considerable decrease in the voltammetric current coupled with positive shift in $E_{1/2}$. The drop of voltammetric currents in the presence of DNA may be attributed to slow diffusion of the metal complex bound to CT DNA. This in turn indicates the extent of binding affinity of the complex to DNA. Finally the conclusion derived from CV study is that the complexes can bind to DNA through intercalative binding mode.

3.9. DNA Cleavage Efficacy

Since there has been a worldwide agreement on the fact that denaturing DNA is the most effective way to stop the multiplication of cancer cells, there have been several methods and procedures that can damage DNA. One such procedure is cleaving of the super coiled DNA using artificial nucleases, and the intention can be achieved by the two pathways, oxidative and hydrolytic cleavage. The oxidative cleavage pathway damages the deoxyribose sugar moieties, whereas the hydrolytic cleavage damages the phosphodiester bonds, considered to be backbone of the DNA mimicking the enzymatic cleavage. Hence, there has been a lot of research in developing metal complexes that mimic the enzymatic reactions. Accordingly, there is a high demand for artificial nucleases (metal complex) which can cleave the super coiled plasmid DNA into nicked form (circular form) or linear form (open circular form) or preferably both.

Therefore, to investigate whether the synthesized complexes can trigger the double strand cleavage of the super coiled plasmid DNA, gel electrophoresis has been carried out. As DNA is negatively charged, it migrates towards the anode when subjected to an electric field. At micromolar concentration at 2 h incubation period, the ligands exhibited

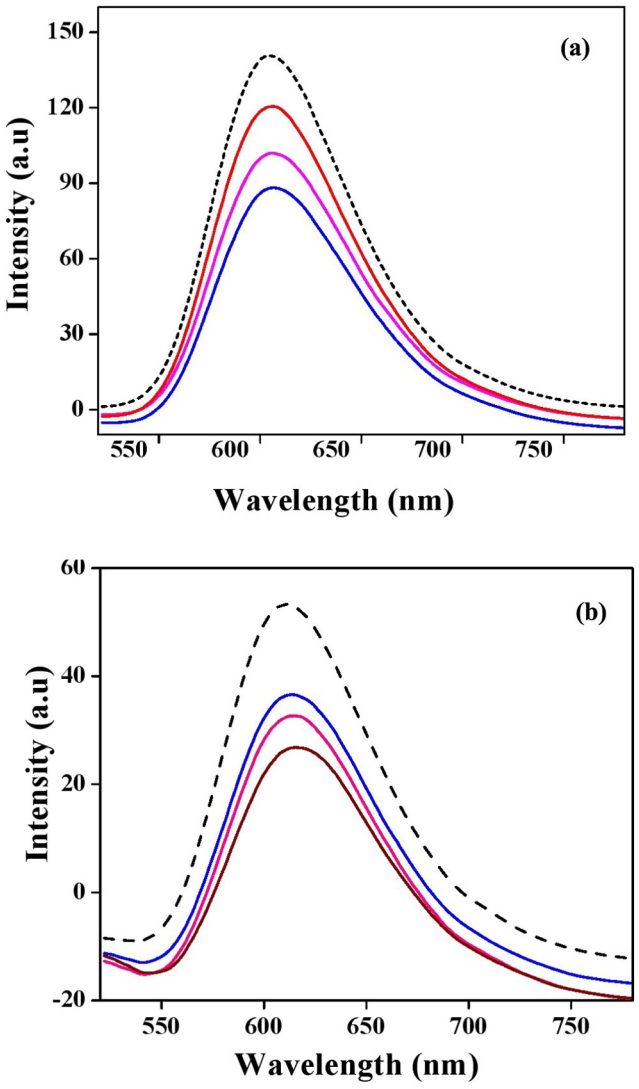

Fig. 3. Emission spectra of EB bound to DNA in the presence of complex **5** (a) and **9** (**b**) ([EB] = 3.3 μM, [DNA] = 20 μM, [complex] = 0–25 μM, λ_{ex} = 500 nm).

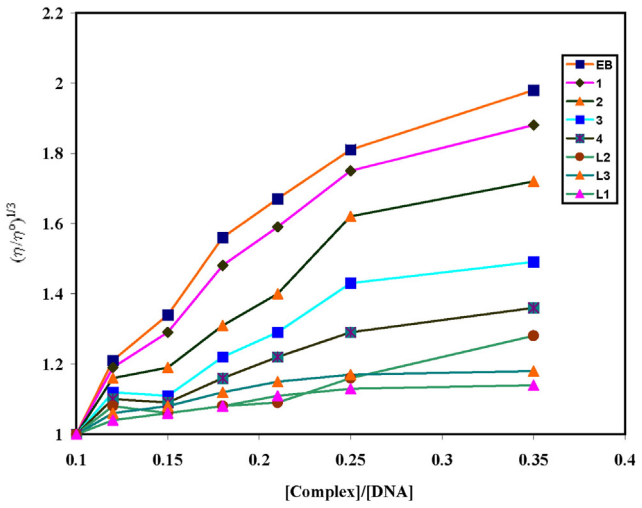

Fig. 4. Effect of increasing amount of [EB] and compounds on the relative viscosity of DNA. 1/R = [Complex]/[DNA] or [EB]/[DNA].

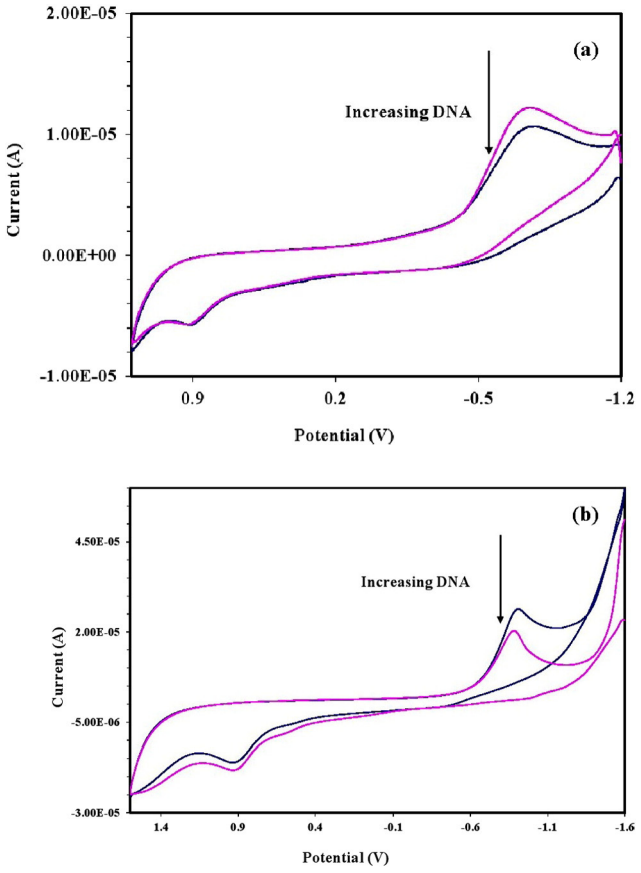

Fig. 5. Cyclic voltammograms of complexes **5** (a) and **9** (b) in buffer pH = 7.2 at 25 °C in the presence of increasing amount of DNA.

moderate cleavage activity in the presence of oxidant (H_2O_2). The activity was greatly enhanced by the incorporation of the metal ion into the respective ligands. The cleavage pattern of DNA in the presence of complexes **5–8** is showed in Fig. 6. No DNA cleavage was observed for the control in which the metal complex was absent (lanes 1, 2) and in the presence of $CuCl_2$ (100 μm) salt. The other lanes containing metal complexes (in form I) are converted into form II and form III. The activity of the complexes was significantly increased in the presence of the oxidant. This may be attributed to the formation of hydroxyl free radicals which oxidize +2 to +3 presumably through Fenton-type reaction, resulting in the formation of reactive oxygen species which could then

Table 3
Redox potential profiles for interaction of DNA with synthesized complexes.

Complexes	[a]ΔEp (V)		[b]$E_{1/2}$ (V)		I_{pa}/I_{pc}
	Free	Bound	Free	Bound	
1	0.355	0.376	0.340	0.346	1.02
2	0.504	0.542	0.212	0.225	0.76
3	0.272	0.278	−0.059	−0.052	0.68
4	0.462	0.494	−0.363	−0.298	0.84
5	0.475	0.562	−0.457	−0.391	1.01
6	−0.291	−0.278	0.342	0.353	1.06
7	0.215	0.297	−1.942	−1.852	0.77
8	−0.421	0.444	−0.462	−0.453	0.81
9	−0.291	−0.278	0.342	0.353	1.04
10	0.355	0.376	0.340	0.346	0.76
11	0.662	0.694	−0.563	−0.498	0.98
12	0.435	0.482	−0.457	−0.391	0.93

Data from cyclic voltammetric measurements: [a]ΔEp = Ep_a − Epc; [b]$E_{1/2}$ is calculated as the average of anodic (E_{Pa}) and cathodic (Ep_c) peak potentials; [b]$E_{1/2} = Ep_a + Epc/2$.

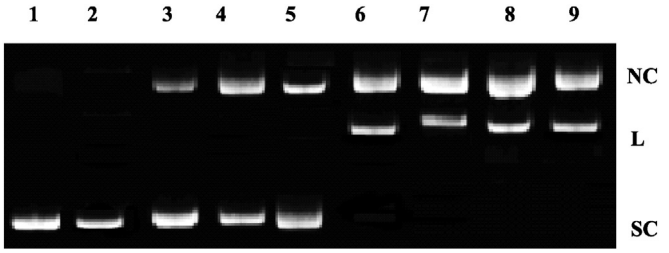

Fig. 6. Gel electrophoresis pattern showing cleavage of pBR322 supercoiled DNA (10 μM) in the presence of H_2O_2 (100 μM). Lane 1: DNA control (10 μM); lane 2: $CuCl_2$ (100 μM); lane 3: DNA + [L^1] (60 μM) + H_2O_2; lane 4: DNA + [L^2] (60 μM) + H_2O_2; lane 5: DNA + [L^3] (60 μM) + H_2O_2; lane 6: DNA + **5** (60 μM) + H_2O_2; lane 7: DNA + 6 (60 μM) + H_2O_2 lane 8: DNA + **7** (60 μM) + H_2O_2; lane 9: DNA + **8** (60 μM) + H_2O_2.

cause hydrolytic damage to DNA [40]. From these results, we infer that all the metal complexes **1–12** act as potential nuclease agents.

3.10. Antimicrobial Activity

With the advent of many diseases and most of them being infectious, the antimicrobial action of the drugs is favored upon. The present scenario of microbes developing resistance to the multiple drugs also insists on inventing new antimicrobial agents with effective pathway to destroy the microbes. Considering this scenario, the triazole Schiff bases (**L^1–L^3**), the metal complexes (**1–12**) and the standards were screened for *in vitro* antimicrobial activity against the five bacterial strains; *Staphylococcus aureus*, *Bacillus subtilis*, *Escherichia coli*, *Klebsiella pneumoniae* and *Salmonella typhi* (Gram-positive and Gram-negative) and fungal strains (*Aspergillus niger*, *Fusarium solani*, *Curvularia lunata*, *Rhizoctonia bataticola*, *Candida albicans*) using the agar-well diffusion method [41].The minimum inhibitory concentration was determined by assaying at several dilutions. In order to evaluate the interfering effect of DMF on the biological screening, alternate studies on DMF solution showed no activity against any microbial strains.

The overall outcome of the screening evidently depicts that all the complexes show higher activity compared to the free ligands. The Overtone's concept [42] and Tweedy's chelation theory [43] efficiently explain the cause of increased activity in the metal complexes. Complex **5** showed highest antimicrobial activity among all the other complexes. The reason pertaining to the presence of electron withdrawing —NO_2 group on the aromatic ring which increases the antimicrobial activities of the tested metal complexes compared to the complexes with electron

Table 4
Minimum inhibitory concentration of the synthesized compounds against growth of bacteria (μM).

Compound	Minimum inhibitory concentration (MIC) (×10^4 μM) SEM = ±2				
	Staphylococcus aureus	*Bacillus subtilis*	*Escherichia coli*	*Klebsiella pneumoniae*	*Salmonella typhi*
L^1	20.3	19.2	19.7	19.3	18.1
L^2	17.7	16.9	16.3	17.4	17.3
L^3	18.0	17.1	17.3	17.7	17.8
1	8.8	9.0	9.2	9.5	9.7
2	10.1	10.4	10.6	10.9	11.2
3	11.5	12.0	12.2	12.5	12.7
4	14.9	15.1	15.3	15.6	15.8
5	7.6	8.0	8.2	8.5	8.7
6	9.2	9.4	9.6	9.9	10.1
7	10.5	10.9	11.1	11.4	11.6
8	12.6	12.8	13.0	13.3	13.5
9	8.4	8.7	8.9	9.2	9.3
10	9.7	10.1	10.3	10.6	10.8
11	10.9	11.3	11.5	11.8	12.0
12	13.8	14.1	14.3	14.6	14.8
[a]Kanamycin	1.6	2.8	1.4	2.3	2.6

[a] Kanamycin is used as the standard.

Table 5
Minimum inhibitory concentration of the synthesized compounds against the growth of fungi (μM).

Compound	Minimum inhibitory concentration (MIC) ($\times 10^4$ μM) SEM = ±2				
	Aspergillus niger	*Fusarium solani*	*Curvularia lunata*	*Rhizoctonia bataticola*	*Candida albicans*
L[1]	20.3	21.6	20.5	18.5	20.4
L[2]	18.2	18.4	17.5	16.9	18.4
L[3]	19.9	19.5	18.6	17.8	19.6
1	9.1	9.8	10.4	9.9	10.7
2	10.2	11.4	11.5	10.2	11.6
3	11.9	12.7	12.8	12.4	12.9
4	13.3	13.6	13.7	13.5	13.9
5	7.8	8.9	8.8	8.2	9.6
6	9.7	10.3	10.8	9.8	10.8
7	10.9	11.8	12.3	10.9	11.9
8	12.4	13.1	13.0	12.8	13.2
9	8.6	9.6	10.3	9.3	9.9
10	10.0	10.9	11.2	10.1	11.4
11	11.7	12.5	12.6	12.1	12.6
12	12.7	13.4	13.6	13.1	13.7
[a]Fluconazole	1.4	1.7	1.2	1.5	1.8

[a] Fluconazole is used as the standard.

donating group as a substituent and complexes having no substituent at all [44].

Moreover, the nature of the metal ion plays a decisive role in determining the antimicrobial properties. Copper, with its redox properties can catalyze the production of highly reactive hydroxyl radicals which can subsequently damage lipids, proteins, DNA and other molecules. This can cause significant disruption in cell membrane (enabling more copper to get through the fungal membrane) leading to extreme damage within the cell. It can be clearly noted from Tables 4 and 5 that complexes **5**, **9** and **1** show much better antibacterial and antifungal activities as compared to other complexes. The order of the activity is given as follows: **5** > **9** > **1** > **6** > **10** > **2** > **7** > **11** > **3** > **8** > **12** > **4**. It is interesting to know that the antimicrobial activity of the present complexes is higher than the previously reported few triazole derived complexes [45,46].

4. Conclusion

The present contribution describes the synthesis of few new transition metal complexes comprising versatile triazole analogues and they have been characterized by analytical and spectral methods. The DNA binding properties of the octahedral complexes have been explored by electronic absorption, fluorescence spectroscopy, cyclic voltammetry and viscosity measurements. The results suggested that all the complexes could interact with CT-DNA through the intercalation fashion and the binding affinities are in the following order: **5** > **9** > **1** > **6** > **10** > **2** > **7** > **11** > **3** > **8** > **12** > **4**. Moreover, the gel electrophoresis investigation discloses that the synthesized compounds are efficient metallonucleases. It is interesting to note that the antimicrobial results reveal the metal complexes are more effective than that of the respective free ligands under identical experimental conditions. All the results point out that the —NO_2 (electron withdrawing group) substituted complexes exhibit prominent activities than the —OCH_3 (electron releasing group) substituted complexes and the unsubstituted complexes. Hence it can be concluded that the —NO_2 substituted complexes may make promising DNA probes and antimicrobial drugs.

Acknowledgments

The authors express their heartfelt thanks to the College Managing Board, Principal and Head of the Department of Chemistry, VHNSN College for providing necessary research facilities. IIT Bombay and CDRI, Lucknow, are gratefully acknowledged for providing instrumental facilities.

Appendix A. Supplementary data

Supplementary data to this article can be found online at http://dx.doi.org/10.1016/j.jphotobiol.2016.02.033.

References

[1] B. Rosenberg, L. VamCamp, J.E. Trosko, V.H. Mansour, Platinum compounds: a new class of potent antitumour agents, Nature 222 (1969) 385–386.
[2] P.R. Chetana, B.S. Srinatha, M.N. Somashekar, R.S. Policegoudra, Synthesis, spectroscopic characterisation, thermal analysis, DNA interaction and antibacterial activity of copper(I) complexes with N,N′-disubstituted thiourea, J. Mol. Struct. 1106 (2016) 352–365.
[3] Z. Wu, Q. Liu, X. Liang, X. Yang, N. Wang, X. Wang, H. Sun, Y. Lu, Z. Guo, Reactivity of platinum-based antitumor drugs towards a Met- and His-rich 20mer peptide corresponding to the N-terminal domain of human copper transporter 1, J. Biol. Inorg. Chem. 14 (2009) 1413–1423.
[4] D.S. Raja, N.S.P. Bhuvanesh, K. Natarajan, A novel water soluble ligand bridged cobalt(II) coordination polymer of 2-oxo-1,2-dihydroquinoline-3-carbaldehyde (isonicotinic) hydrazone: evaluation of the DNA binding, protein interaction, radical scavenging and anticancer activity, Dalton Trans. 41 (2012) 4365–4377.
[5] X. Qiao, Z.Y. Ma, C.Z. Xie, F. Xue, Y.W. Zhang, J.Y. Xu, Z.Y. Qiang, J.S. Lou, G.J. Chen, S.P. Yan, Study on potential antitumor mechanism of a novel Schiff base copper(II) complex: synthesis, crystal structure, DNA binding, cytotoxicity and apoptosis induction activity, J. Biol. Inorg. Chem. 105 (2011) 728–737.
[6] P.J. Bednarski, F.S. Mackay, P.J. Sadler, Photoactivatable platinum complexes, Anti Cancer Agents Med. Chem. 7 (2007) 75–93.
[7] I. Machado, M. Fernández, L. Becco, B. Garat, R.F. Brissos, N. Zabarska, P. Gamez, F. Marques, I. Correia, J. Costa Pessoa, D. Gambino, New metal complexes of NNO tridentate ligands: effect of metal center and co-ligand on biological activity, Inorg. Chim. Acta 420 (2014) 39–46.
[8] P. Banerjee, O.P. Pandey, S.K. Sengupta, Microwave assisted synthesis, spectroscopic and antibacterial studies of titanocene chelates of Schiff bases derived from 3-substituted-4-amino-5-hydrazino-1,2,4-triazoles, Transit. Met. Chem. 33 (2008) 1047–1052.
[9] G.T. Zitouni, Z.A. Kaplancikli, M.T. Yildiz, P. Chevallet, D. Kaya, Synthesis and antimicrobial activity of 4-phenyl/cyclohexyl-5-(1-phenoxyethyl)-3-[N-(2-thiazolyl) acetamido] thio-4H-1,2,4-triazole derivatives, Eur. J. Med. Chem. 40 (2005) 607–613.
[10] S.B. Deepthi, P. Ramesh, R. Trivedi, S.K. Buddana, R.S. Prakasham, Carbohydrate triazole tethered 2-pyridyl-benzimidazole ligands: synthesis of their palladium (II) complexes and antimicrobial activities, Inorg. Chim. Acta 435 (2015) 200–205.
[11] M.S. Karthikeyan, D.J. Prasad, B. Poojary, K.S. Bhat, B.S. Holla, N.S. Kumari, Synthesis and biological activity of Schiff and Mannich bases bearing 2,4-dichloro-5-fluorophenyl moiety, Bioorg. Med. Chem. 14 (2006) 7482–7489.
[12] Z. Rezaei, S. Khabnadideh, K. Pakshir, Z. Hossaini, F. Amiri, E. Assadpour, Design, synthesis and antifungal activity of triazole and benzotriazole derivatives, Eur. J. Med. Chem. 44 (2009) 3064–3067.
[13] A.K. Sadana, Y. Mirza, K.R. Aneja, O. Prakash, Hypervalent iodine mediated synthesis of 1-aryl/hetryl-1,2,4-triazolo[4,3-a] pyridines and 1-aryl/hetryl 5-methyl-1,2,4-triazolo[4,3-a]quinolines as antibacterial agents, Eur. J. Med. Chem. 38 (2003) 533–536.
[14] K. Singh, Antibacterial Co(II), Ni(II), Cu(II) and Zn(II) complexes of Schiff bases derived from fluorobenzaldehyde and triazoles, J. Enzym. Inhib. Med. Chem. 21 (2006) 557–562.
[15] G.B. Bagihalli, S.A. Patil, Synthesis, spectral characterization, *in vitro* biological and DNA cleavage studies of Co(II), Ni(II), Cu(II), and Zn(II) complexes with 1,2,4-triazole Schiff bases, J. Coord. Chem. 62 (2009) 1690–1700.
[16] H. Guo-Qiang, H. Li-Li, X. Song-Qiang, H. Wen-Long, Design, synthesis and antitumor activity of asymmetric bis(s-triazole Schiff-base) bearing functionalized side-chain, Chin. J. Chem. 26 (2008) 1145–1149.
[17] O. Bekircan, N. Gumrukcuoglu, Synthesis of some 3,5-diphenyl-4H-1,2,4-triazole derivatives as antitumor agents, Ind. J. Chem. 44 (2005) 2107–2113.
[18] E. De Clercq, Antiviral drugs in current clinical use, J. Clin. Virol. 30 (2004) 115–133.
[19] L. Navidpour, H. Shadnia, H. Shafaroodi, M. Amini, A.R. Dehpour, A. Shafiee, Design, synthesis and biological evaluation of substituted 2-alkylthio-1,5-diarylimidazoles as selective COX-2 inhibitors, Bioorg. Med. Chem. 15 (2007) 1976–1982.
[20] Y. Naito, F. Akahoshi, S. Takeda, T. Okada, M. Kajii, H. Nishimura, M. Sugiura, C. Fukaya, Y. Kagitani, Synthesis and pharmacological activity of triazole derivatives inhibiting eosinophilia, J. Med. Chem. 39 (1996) 3019–3029.
[21] A. Almasirad, S.A. Tabtabai, M. Faizi, A. Kebtiaeezadeh, N. Mehrabhi, A. Daivandi, A. Shafiee, Synthesis and anticonvulsant activity of new 2-substituted-5-{2-(2-fluorophenoxy)phenyl}-1,3,4-oxadiazoles and 1,2,4-triazoles, Bioorg. Med. Chem. Lett. 14 (2004) 6057–6059.
[22] J. Jin, L. Zhang, A. Zhang, X.X. Lei, J.H. Zhu, Synthesis and biological activity of some novel derivatives of 4-amino-3-(D-galactopentitol-1-yl)-5-mercapto-1,2,4-triazole, Molecules 12 (2007) 1596–1605.
[23] G.B. Bagihalli, P.G. Avaji, S.A. Patil, P.S. Badami, Synthesis, spectral characterization, in vitro antibacterial, antifungal and cytotoxic activities of Co(II), Ni(II) and Cu(II) complexes with 1,2,4-triazole Schiff bases, Eur. J. Med. Chem. 43 (2008) 2639–2649.
[24] O. Bekircan, H. Bektas, Synthesis of new bis-1,2,4-triazole derivatives, Molecules 11 (2006) 469–477.
[25] W.G. Geary, The use of conductivity measurements in organic solvents for the characterisation of coordination compounds, Coord. Chem. Rev. 7 (1971) 81–122.

[26] E. Labisbal, L. Rodriguez, A. S–Pedarares, M. Alonso, A. Vizoso, J. Romero, J.A. Garcia–Vazequez, A. Sousa, Synthesis, characterisation and X-ray structures of diorganotin(IV) and iron(III) complexes of dianionic terdentate Schiff base ligands, J. Organomet. Chem. 691 (2006) 1321–1332.
[27] A.B.P. Lever, Inorganic Electronic Spectroscopy, second ed. Elsevier, Amsterdam, The Netherlands, 1984.
[28] A.B.P. Lever, Inorganic Electronic Spectroscopy, second ed. Elsevier, New York, 1968.
[29] F.A. Cotton, G. Wilkinson, Advanced Inorganic Chemistry, fifth ed. Wiley, New York, 1988.
[30] S.S. Konstantinovic, B.C. Radovanovic, A. Krkljes, Antimicrobial activity of some isatin-3–thiosemicarbazone complexes, J. Therm. Anal. Calorim. 90 (2007) 525–531.
[31] N. Raman, K. Pothiraj, T. Baskaran, DNA interaction, antimicrobial, electrochemical and spectroscopic studies of metal(II) complexes with tridentate heterocyclic Schiff base derived from 2′-methylacetoacetanilide, J. Mol. Struct. 1000 (2011) 135–144.
[32] R. K. Ray and G.B. Kauffman, EPR spectra and covalency of bis(amidinourea/O-alkyl-1-amidinourea)copper(II) complexes part II. Properties of the CuN_4^{2-} chromophore, Inorg. Chim. Acta. 173 (1990) 207–214.
[33] D.X. West, 2-Aminopyridine n-oxide complexes formed from various copper(II) salts, Inorg. Nucl. Chem. 43 (1984) 3169–3174.
[34] N. Shahabadi, M. Falsafi, N.H. Moghadam, DNA interaction studies of a novel Cu(II) complex as an intercalator containing curcumin and bathophenanthroline ligands, J. Photochem. Photobiol. B 122 (2013) 45–51.
[35] C.N.N′soupkpoe Kossi, C. Descoteaux, E. Asselin, H.A.T. Riahi, G. Berube, DNA interaction with novel antitumor estradiol-platinum(II) hybrid molecule: a comparative study with cisplatin drug, Cell Biol. 27 (2008) 101–107.
[36] C. Rajarajeswari, R. Loganathan, M. Palaniandavar, E. Suresh, A. Riyasdeen, M.A. Akbarsha, Copper(II) complexes with 2NO and 3N donor ligands: synthesis, structures and chemical nuclease and anticancer activities, Dalton Trans. 42 (2013) 8347–8363.
[37] S. Mahadevan, M. Palaniandavar, Spectroscopic and voltammetric studies on copper complexes of 2,9-dimethyl-1,10-phenanthrolines bound to calf thymus DNA, Inorg. Chem. 37 (1998) 693–700.
[38] S.S. Zhang, S.Y. Niu, B. Qu, G.F. Jie, H. Xu, C.F. Ding, Studies on the interaction mechanism between hexakis(imidazole) manganese(II) terephthalate and DNA and preparation of DNA electrochemical sensor, J. Inorg. Biochem. 99 (2005) 2340–2347.
[39] M.T. Carter, M. Rodriguez, A.J. Bard, Voltammetric studies of the interaction of metal chelates with DNA. 2. tris-chelated complexes of cobalt(III) and iron(II) with 1,10-phenanthroline and 2,2′-bipyridine, J. Am. Chem. Soc. 111 (1989) 8901–8911.
[40] A.S. Munde, A.N. Jagdale, S.M. Jadhow, T.K. Chondhekar, Synthesis and characterization of some transition metal complexes of unsymmetrical tetradentate Schiff Base ligand, J. Korean Chem. Soc. 53 (2009) 407–414.
[41] A.U. Rahman, M.I. Choudhary, W.J. Thomsen, Bioassay Techniques for Drug Development, Harwood Academic Publishers, The Netherlands, 2001.
[42] R. Ramesh, S. Maheswaran, Synthesis, spectra, dioxygen affinity and antifungal activity of Ru(III) Schiff base complexes, J. Inorg. Biochem. 96 (2003) 457–462.
[43] Y. Anjaneyulu, R.P. Rao, Preparation, characterization and antimicrobial activity studies on some ternary complexes of Cu(II) with acetylacetone and various salicylic acids, Synth. React. Inorg. Met. Org. Chem. 16 (1986) 257–272.
[44] N.N. Al-Mohammed, Y. Alias, Z. Abdullah, R.M. Shakir, E.M. Taha, A.A. Hamid, Synthesis and antibacterial evaluation of some novel imidazole and benzimidazole sulfonamides, Molecules 18 (2013) 11978–11995.
[45] H. Khanmohammadi, M.H. Abnosi, A. Hosseinzadeh, M. Erfantalab, Synthesis, biological and computational study of new Schiff base hydrazones bearing 3-(4-pyridine)-5-mercapto-1,2,4-triazole moiety, Spectrochim. Acta 71 (A) (2008) 1474–1480.
[46] A.J. Bard, L.R. Izatt (Eds.), Electrochemical Methods: Fundamentals and Applications, second ed. Wiley, New York, 2001.